Wilkin, J., W. G. Zhang, B. Cahill and R. C. Chant (2011), Integrating coastal models and observations for studies of ocean dynamics, observing systems and forecasting, In Operational Oceanography in the 21st Century, A. Schiller and G. Brassington (eds.), Springer, pp 487-512, doi:10.1007/978-94-007-0332-2_19

Chapter 19
Integrating Coastal Models and Observations for Studies of Ocean Dynamics, Observing Systems and Forecasting

John L. Wilkin, Weifeng G. Zhang, Bronwyn E. Cahill and Robert C. Chant

Abstract In coastal oceanography, simulation models are used to a variety of ends. Idealized studies may address particular dynamical processes or features of coastline and bathymetry; reproducing the circulation in a geographical region can compliment studies of ecosystems and geomorphology; and models may be employed to simulate observing systems and to forecast oceanic conditions for practical operational needs. Frequently, the interplay between multiple forcing mechanisms, geographic detail, stratification, and nonlinear dynamics, is significant, and this demands that ocean models for coastal applications are capable of representing a comprehensive suite of dynamical processes. Drawing on a series of recent model-based studies of the inner to mid-shelf region of the Middle Atlantic Bight (MAB) we illustrate, by example, these methodologies and the breadth of dynamical processes that influence coastal ocean circulation. We demonstrate that the recent introduction of variational methods into coastal ocean simulation is a development that greatly enhances our ability to integrate models with data from the evolving coastal ocean observatories for the purposes of improved ocean prediction, adaptive sampling and observing system design.

19.1 Introduction

The discharge of rivers to continental shelf seas represents an important mechanism by which human activities in urban watersheds impact the neighbouring marine environment. Biogeochemical, sediment, and ecosystem processes that determine the ultimate fate of nutrients and pollutants delivered into the coastal ocean by river sources depends on the pathways and time scales of dispersal of these buoyant discharges. How coastal models, in conjunction with observations, can be used to study these circulation processes is illustrated here by example, by reviewing results

J. L. Wilkin (✉)
Institute of Marine and Coastal Sciences, Rutgers, The State University of New Jersey, New Brunswick, NJ, USA
e-mail: jwilkin@rutgers.edu

A. Schiller, G. B. Brassington (eds.), *Operational Oceanography in the 21st Century,*
DOI 10.1007/978-94-007-0332-2_19,

from a recent series of model-based studies of the Hudson River outflow into New York Bight.

On many coasts, the flux of freshwater from rivers or groundwater first enters an estuary where it mixes with more salty waters of oceanic origin before reaching the adjacent shelf sea. The salinity of the estuary discharge can be sufficiently low that horizontal buoyancy gradients are a significant force influencing the plume circulation. A classical view of the ensuing dynamics is that the buoyancy force balances the Coriolis force, and the outflow turns to the right (in the northern hemisphere) and forms a narrow coastal current a few internal Rossby radii in width trapped against the coast. If the front that defines the outer extent of the low salinity water reaches the sea floor then the plume becomes bottom-attached and details of the coastal bathymetry strongly influence the plume trajectory. Alternatively, if the low salinity discharge is confined to a relatively thin surface layer the plume is described as surface-advected (Yankovsky and Chapman 1997) and may be more responsive to local wind forcing. Whether a plume falls into the surface-advected or bottom-trapped regime, or transitions from one regime to the other, depends on river discharge, bathymetry, and mixing within the surface and bottom boundary layers.

It is often the case that the freshwater transport of the coastal current is less than the freshwater flux out of the estuary, particularly during episodes of elevated river discharge, and this leads to the formation of a pronounced low salinity bulge near the estuary outflow. The across shelf scale of the bulge can be several times the width of the coastal current, especially for a surface-advected plume. The low buoyancy of the bulge evolves an anti-cyclonic circulation that significantly prolongs the duration that water discharged from the estuary is retained in the vicinity of the estuary mouth. Laboratory rotating tank experiments have shown that the coastal current can receive as little as one third of the estuary outflow (Avicola and Huq 2003), or in extreme circumstances the recirculation can pinch off from the coastal current and for a period of time direct all flow into the bulge (Horner-Devine et al. 2006). Numerical model studies show that the ratio of coastal current transport to estuary discharge decreases as the flow becomes increasingly non-linear as characterized by the Rossby number, i.e. the ratio of inertial to rotational forces (Fong and Geyer 2002; Nof and Pichevin 2001).

Thus river flow rate, vertical turbulent mixing within the estuary and on the shelf, bathymetric detail, stratification, non-linear dynamics, and wind forcing are all factors that influence river plume dispersal characteristics. Shelf-wide alongshelf mean currents established by regional winds (Fong and Geyer 2002) or by upstream or offshore remote forcing further influence the circulation (Zhang et al. 2009a). Consequently, ocean models that seek to simulate interactions between river discharges and the adjacent inner shelf must be quite comprehensive in the suite of dynamical processes that they represent.

In this article we demonstrate the capabilities of one such model, the Regional Ocean Modelling System (ROMS; www.myroms.org), by summarizing results from a sequence of studies of the Hudson River's discharge into the coastal ocean based on efforts during the Lagrangian Transport and Transformation Experiment (LaTTE) (Chant et al. 2008). The Hudson River watershed is highly industrialized, and the LaTTE field program included observations—following the river plume associated with the spring freshest in the years 2004, 2005 and 2006—of phytoplankton and zooplankton assemblages, and natural and human-source nutrients, organic matter, and metal contaminants. An emphasis of the project was to investigate how the plume's physical structure influenced biogeochemical processes. Key processes in this regard include mixing that dilutes salinity and influences certain chemical reactions, light levels that affect photochemistry, and residence times and transport pathways that can impact rates of bioaccumulation and modify where regions of net export of particulate suspended matter might occur.

Dynamical and computational features of ROMS that are pertinent to the LaTTE simulations (and coastal processes in general) are described in Sect. 19.2, and revisited in Sect. 19.4 in a discussion of aspects of New York Bight (NYB) regional dynamics worthy of further analysis. Section 19.3 describes modelling approaches we have taken to address specific scientific objectives. Section 19.3.1 considers forward simulations initialized from climatology and forced with observed river flows and an atmospheric forecast model used for short-term forecasting for adaptive sampling during the LaTTE field experiments, and idealized studies of how the plume responds to the wind. Multi-year simulations to examine long-term transport and dispersal pathways, and the mean dynamics of the circulation, are presented in Sect. 19.3.2. Section 19.3.3 describes a reanalysis of the 2006 LaTTE season using Incremental Strong Constraint 4-Dimensional Variational Data Assimilation (IS4DVAR) to adjust initial conditions to each daily forecast cycle, and gives a brief overview of how variational methods might also be employed to assist observing system operation. In Sect. 19.5 it is summarized how the studies described here collectively illustrate how coastal models are being increasingly integrated with the growing network of regional coastal ocean observing systems to better understand coastal ocean processes, and improve ocean predictions.

19.2 Regional Ocean Modelling System

19.2.1 Dynamical and Numerical Core

ROMS solves the hydrostatic, Boussinesq, Reynolds-averaged Navier-Stokes equations in terrain-following vertical coordinates. It employs a split-explicit formulation whereby the 2-dimensional continuity and barotropic momentum equations are advanced using a much smaller time step than the 3-dimensional baroclinic momentum and tracer equations.

The ROMS computational kernel is described elsewhere (Shchepetkin and McWilliams 2005, 2009a, b) and will not be detailed here, but we do note several aspects of the kernel that are particularly attractive for coastal ocean simulation. These include a formulation of the barotropic mode equations that accounts for the non-uniform density field so as to reduce aliasing and coupling errors associated with the split-explicit method (Higdon and de Szoeke 1997) in terrain-following coordinates. Temporal-weighted averaging of the barotropic mode prevents aliasing of unresolved signals into the slow baroclinic mode while accurately representing barotropic motions resolved by the baroclinic time step (e.g. tides and coastal-trapped waves). Several features of the kernel substantially reduce pressure-gradient force truncation error that has been a long-standing problem in terrain following coordinate ocean models. A finite-volume, finite-time-step discretization for the tracer equations improves integral conservation and constancy preservation properties associated with the variable free surface, which is important in coastal applications where the free surface displacement represents a significant fraction of the water depth. A positive-definite MPDATA (multidimensional positive definite advection transport algorithm) advection scheme (Smolarkiewicz 1984) is available, which is attractive for biological tracers and sediment concentration. A monotonized, high-order vertical advection scheme for sinking of sediments and biological particulate matter integrates depositional flux over multiple grid cells so it is not constrained by the CFL criterion (Warner et al. 2008a).

Interested readers are referred to Shchepetkin and McWilliams (2009b) for a thorough review of the choices of algorithmic elements that make ROMS particularly accurate and efficient for high-resolution simulations in which advection is strong, and currents, fronts and eddies are approximately geostrophic—characteristics of mesoscale processes in the coastal ocean and adjacent deep sea.

19.2.2 Vertical Turbulence Closure

ROMS provides users with several options for the calculation of the vertical eddy viscosity for momentum and eddy diffusivity for tracers. In the majority of recent ROMS coastal applications the choice of vertical turbulence-closure formulation has been either (1) a k-profile parameterization (KPP) for both surface and bottom-boundary layers (Large et al. 1994; Durski et al. 2004), (2) Mellor-Yamada level 2.5 (MY25) (Mellor and Yamada 1982), or (3) the generic length-scale (GLS) method (Umlauf and Burchard 2003) which encompasses a suite of closure and stability function options.

The KPP scheme specifies turbulent mixing coefficients in the boundary layers based on Monin-Obukhov similarity theory, and in the interior principally as a function of the local gradient Richardson number (Large et al. 1994; Wijesekera et al. 2003). The KPP method is diagnostic in the sense it does not solve a time evolving (prognostic) equation for any of the elements of the turbulent closure, whereas the MY25 and GLS schemes are of the general class of closures where two prognostic equations are solved—one for turbulent kinetic energy and the other related to turbulence length scale.

Warner et al. (2005) describe the implementation of the GLS formulation in ROMS, and contrast the performance of the various GLS sub-options (representing different treatments of the turbulent length scale) and the historically widely used MY25 scheme. They find that the differing schemes lead to differences in the vertical eddy mixing profiles, but the net impact on profiles of model state variables (velocities and tracers) is relatively minor. Wijesekera et al. (2003) reach similar conclusions, but note that results for KPP tend to be less similar to GLS and MY25, which are quite alike. Warner et al. (2005) found that suspended sediment concentrations in their sediment transport model are much more sensitive to the choice of closure than is salinity in estuarine mixing simulations. In the LaTTE simulations we use the GLS *k-kl* closure option, which is essentially an implementation of MY25 within the GLS conceptual framework.

19.2.3 Forcing

19.2.3.1 Air-Sea Fluxes

Air-land-sea contrasts, orography, upwelling, fog, and tidal mixing over variable bathymetry in the coastal ocean can all contribute to creating wind and air temperature conditions at sea level that have much shorter time and length scales than typically occur further offshore or in the open ocean. Accordingly, coastal ocean simulations benefit from the availability of spatially and temporally well-resolved meteorological forcing and accurate parameterization of air-sea momentum and heat fluxes.

Surface atmospheric forcing in the LaTTE simulations made use of two sets of marine boundary layer products derived from atmospheric models. The short time scale simulations (Sect. 19.3.1) and IS4DVAR reanalysis (Sect. 19.3.3) used marine boundary conditions (downward long-wave radiation, net shortwave radiation, 10-m wind, 2-m air temperature, pressure and humidity) at 3-hourly intervals from the North American Mesoscale model (NAM; Janjic 2004)—a 12 km resolution 72-h forecast system operated by the National Centers for Environmental Prediction (NCEP). The multiyear simulations (Sect. 19.3.2) used marine boundary layer conditions taken from the North American Regional Reanalysis (Mesinger 2006)—a 25-km resolution 6-hourly interval data assimilative reanalysis product. Air-sea fluxes of momentum and heat were computed using standard bulk formulae (Fairall et al. 2003) from the atmospheric model based marine boundary layer conditions in conjunction with the sea surface temperature from ROMS.

19.2.3.2 River Inflows and Open Boundary Conditions

In coastal Regions of Freshwater Influence (ROFI) (Hill 1998), lateral buoyancy input from rivers produces density gradients that are principally horizontal, which leads to relatively weak vertical stability compared to the vertical stratification generated from comparable surface air-sea buoyancy fluxes. Density stratification in ROFI subsequently arises from the baroclinic adjustment of these density gradients, and destratification and restratification can occur rapidly in response to changing rates of vertical mixing associated with wind forcing and tides (which may have significant spring-neap variability in intensity).

On some coasts, groundwater discharge directly to the coastal ocean or freshwater input from numerous small streams and rivers can be significant, but in the NYB terrestrial buoyancy input is overwhelmingly from large rivers, and predominantly from the Hudson. For river input to the LaTTE model we used daily average observations of river discharge from U.S. Geological Survey gauging stations on the Hudson and Delaware rivers, modified to include ungauged portions of the watershed following Chant et al. (2008).

At the open boundaries to the LaTTE model domain, simple Orlanski-type radiation conditions were applied to tracers (temperature and salt) and 3-D velocity. Our emphasis here on the buoyancy driven circulation associated with the Hudson River plume allows this simplification with its implicit neglect of the influence of remote sources of freshwater and heat. Open boundary sea level and depth-averaged velocity variability was set using the Chapman (1985) and Flather (1976) schemes to radiate surface gravity waves while also imposing tidal harmonic velocity variability derived from a regional tide model (Mukai et al. 2002). In the long multiyear simulations (Sect. 19.5), the boundary depth averaged velocity was augmented with the estimate of mean southwestward current on the shelf derived by Lentz (2008) based on long-term current-meter observations and momentum balance arguments.

19.2.4 Sub-Models for Interdisciplinary Studies

ROMS incorporates a set of sub-models for interdisciplinary applications that are integrated with the dynamical kernel. Among these are several ecosystem models formulated in terms of Eulerian functional groups wherein 3-D tracers representing nutrients, plankton, zooplankton, detritus, etc., expressed in terms of some common currency (usually equivalent nitrogen concentration), are advected and mixed according to the same transport equations as the dynamic tracers. Haidvogel et al. (2008) give an overview of examples of these models, which range in complexity from a four component nitrogen-based (NPZD) model (Powell et al. 2006; Moore et al. 2009) to a carbon based bio-optical model (EcoSim) (Bissett et al. 1999; Cahill et al. 2008) with a spectrally resolved light field and more than 60 state variables representing four phytoplankton, five pigments, five elements, bacteria, dissolved organic matter, and detritus.

A Community Sediment Transport Model (CSTM; Warner et al. 2008a) and wave model (SWAN, Surface Waves in the Nearshore; Booij et al. 1999) are integrated with ROMS for studies of sediment dynamics and circulation in nearshore environments; wave radiation stresses are included in the momentum equations and wave-current interaction that enhances bottom stress is included in the bottom boundary layer dynamics. A user-defined set of non-cohesive sediment classes is tracked, with differential erosion and deposition of the various size classes contributing to the evolution of a multi-level sediment bed with varying layer thickness, porosity, and mass, which allows computation of bed morphology and stratigraphy. The application of the ROMS/SWAN/CSTM to studies of sediment morphology, sorting and transport in an idealized tidal inlet and Massachusetts Bay are presented by Warner et al. (2008a).

19.3 ROMS Simulations of the New York Bight Region for LaTTE

19.3.1 Dispersal of the Plume During High River Discharge

The ROMS model domain for LaTTE (Fig. 19.1) extends from south of Delaware Bay to eastern Long Island, and from the New Jersey and New York coasts to roughly the 70-m isobath. The model has 30 vertical layers and horizontal grid resolution is 1 km.

In spring 2005 and 2006 the model was used to forecast circulation in the NYB in support of LaTTE field observation programs (Foti 2007). Figure 19.2 shows vis-

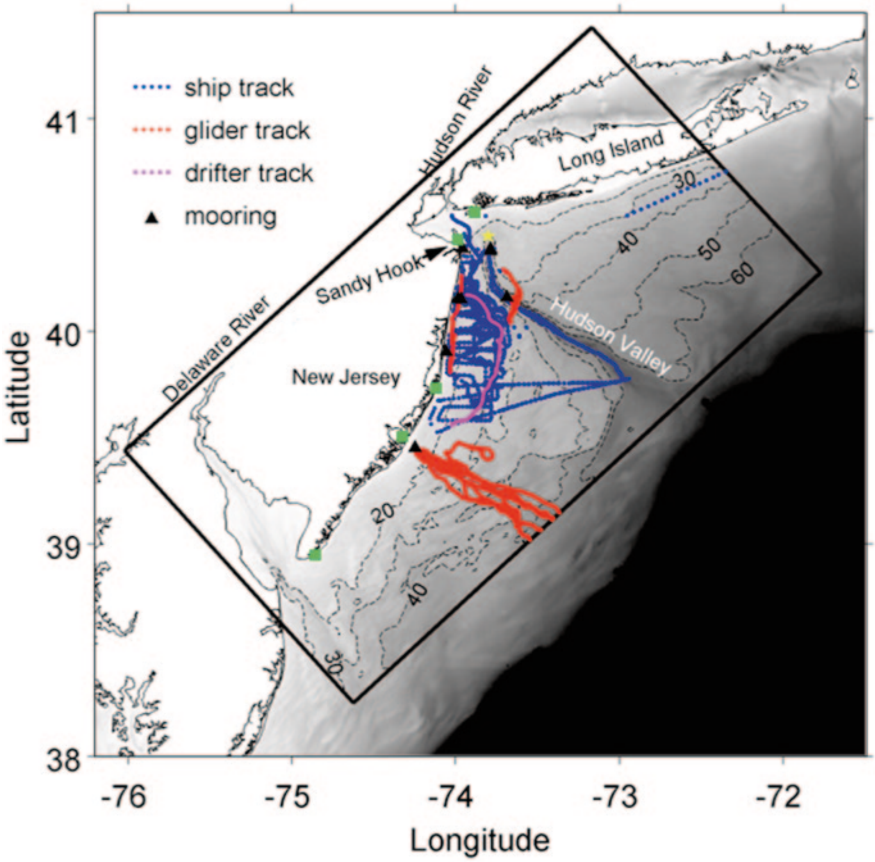

Fig. 19.1 The model domain (*black line*) and locations of observations used in the 4DVAR data assimilation (Sect. 19.3.4). Bathymetry of the New York Bight is in *greyscale; black dash lines* are model isobaths in metres; *yellow star* in the location of Ambrose Tower; *green squares* indicate the five HF radar stations

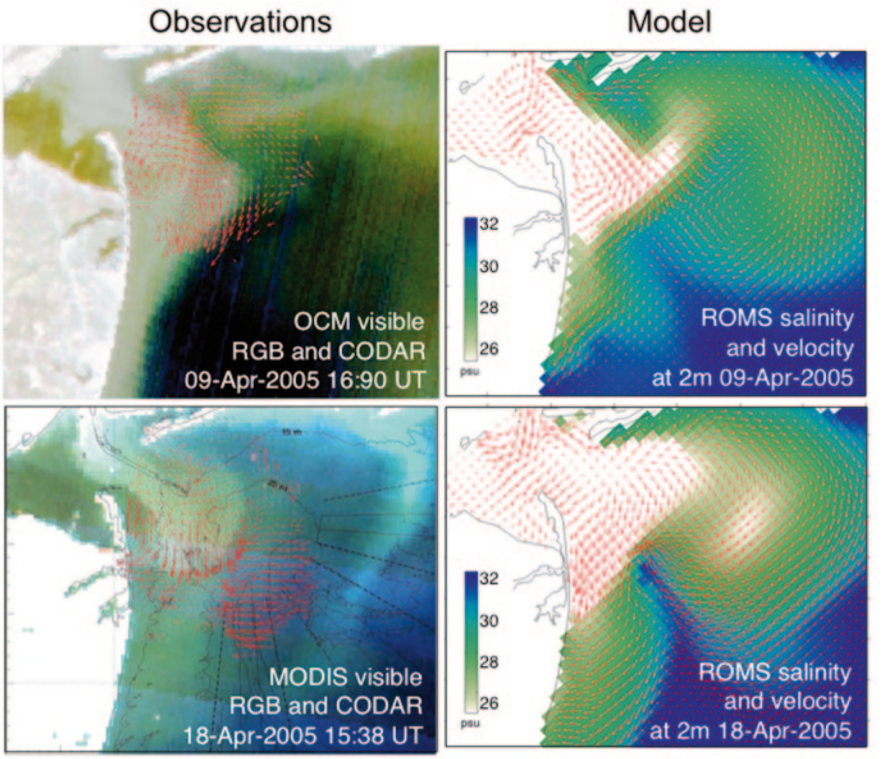

Fig. 19.2 *Left*: Visible imagery from Ocean Colour Monitor (OCM) instrument aboard Indian IRS-P4 satellite, and MODIS instrument aboard NASA Terra satellite showing turbid waters associated with the Hudson River discharge, and vectors of surface current from HF radar (CODAR), on two days during the spring 2005 LaTTE experiment. *Right*: Modelled surface salinity and currents at the corresponding times

ible satellite imagery of the Hudson River plume as it enters the NYB on two days in 2005 overlaid with vectors showing surface current observed by HF-radar, and the modelled velocity and surface salinity and corresponding time—surface salinity being a proxy for the signature of the river source waters. A recirculating bulge of low salinity water is being over-run by a renewed ebb tide discharge of Hudson River estuary waters. Figure 19.3 compares satellite observed absorption at wavelength 488 nm from Oceansat-1 (a proxy for relative chlorophyll abundance and the presence of river source water) with the modelled equivalent freshwater thickness $\delta_{fw} = \int_{-h}^{\zeta} (S_o - S(z))/S_o\, dz$, where S is salinity, h is the water depth, and $z = \zeta$ is the sea surface. If it were possible to locally "unmix" the water column into two layers of salinities zero and S_o, the thickness of the fresh water layer would be δ_{fw}. This depicts the horizontal extent of freshwater dispersal more faithfully than sea surface salinity. Here we use a reference salinity $S_o = 32$.

Figures 19.2 and 19.3, and further model-data comparisons in Zhang et al. (2009a), indicate that fundamental features of the river plume circulation such as the across and along-shelf length scales, the extent of the freshwater bulge, veloc-

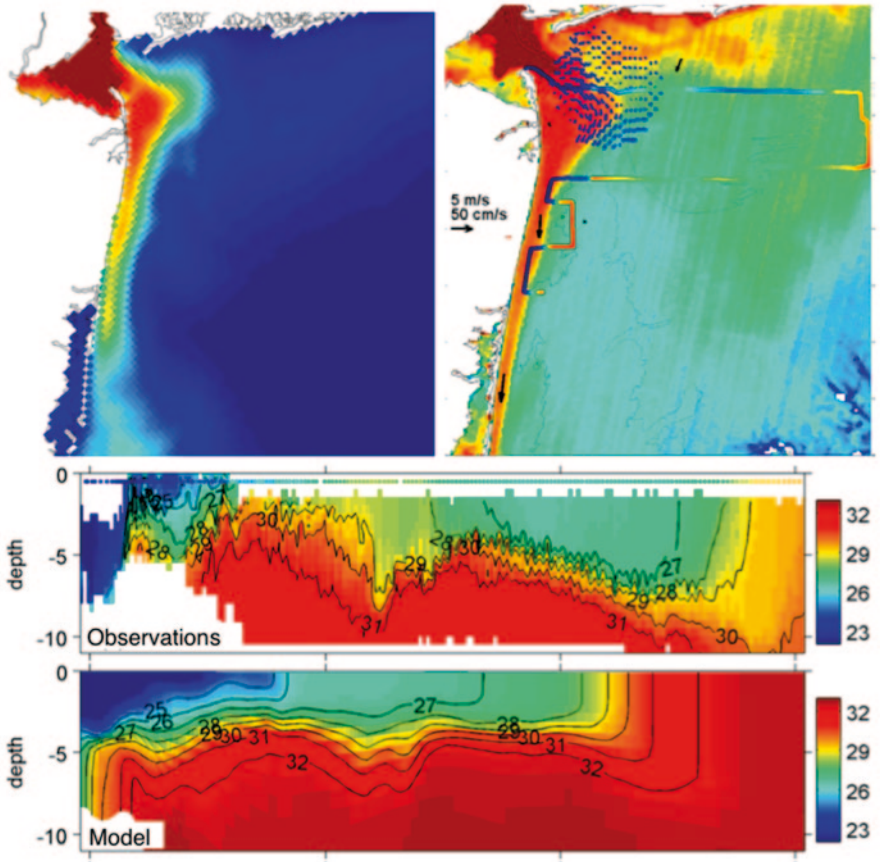

Fig. 19.3 *Top row*: Modelled equivalent freshwater thickness in meters (*left*) and satellite observed absorption at wavelength 488 nm from Oceansat-1 (*right*) showing the patterns of influence of Hudson River source waters. *Bottom*: Observed and modelled salinity along the northernmost west-east transect indicated in the *top right* panel

ity patterns, and the transport pathway from the harbor to the coastal current, are similar in model and observations.

Figure 19.4 shows the time evolution of simulated equivalent freshwater thickness during the spring freshet of 2005. From 1 to 7 April the river discharge exceeded 2,500 m^3/s, or more than four times the annual mean, and peaked at 6,500 m^3/s on 4 April. Initially, southward downwelling favourable winds drive the river plume rapidly southward along the New Jersey coast, but this flow is abruptly arrested on 4 April with the onset of northward upwelling favourable winds. This causes the river flow during peak discharge to form a large low-salinity recirculating bulge located predominantly on the northern side of the Hudson Shelf Valley. From 10 to 15 April a period of weak and variable winds associated with the sea breeze phenomenon enable the bulge to partially drain into a New Jersey coastal current. The return of upwelling winds on April 17 drives more low salinity water eastward and detaches the bulge

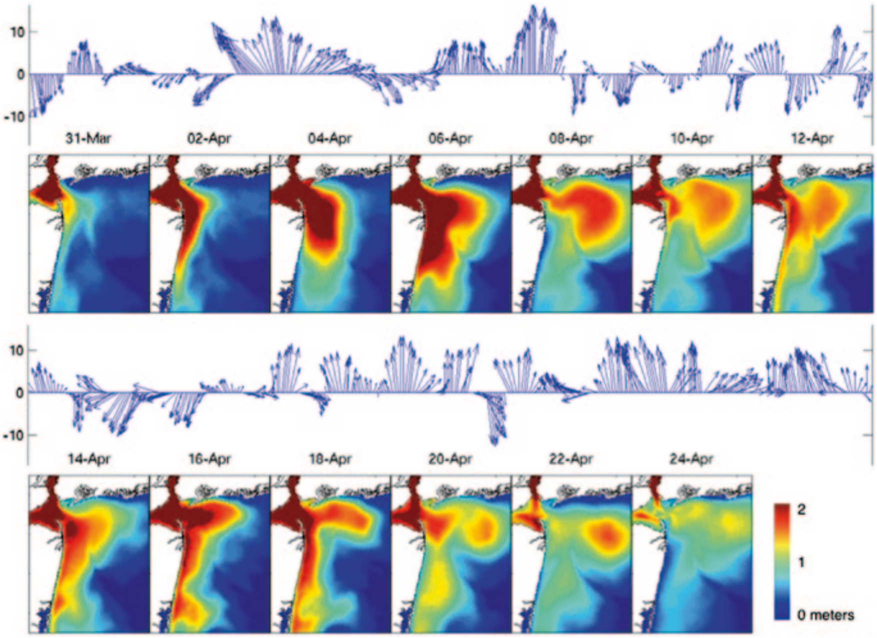

Fig. 19.4 Modelled equivalent freshwater thickness in meters during the spring freshet of 2005 and winds observed at Ambrose Tower in the New York Bight apex

from the estuary discharge that previously fed it. In the week that follows, sustained winds further disperse the plume as the river discharge drops and the freshet ends.

The influence of wind direction and strength on Hudson River plume dispersal has been considered in some detail (Choi and Wilkin 2007) using the same model but for idealized winds and freshet river discharge. Figure 19.5 contrasts the plume behaviour commencing from the same initial conditions (Fig. 19.5a) in response to winds from differing directions (Fig. 19.5d–g) sustained for 3 days. The sensitivity described for the April 2005 simulations is confirmed. Southward winds, and to a lesser extent eastward winds, favour New Jersey coastal current formation. Northward winds eliminate the buoyancy-driven coastal current, disperse the bulge eastward and drive flow along the Long Island coast. Westward winds hamper the discharge from the Hudson River estuary, leading to a build up of low salinity water in New York Harbor. In the absence of wind forcing, the low salinity bulge continues to grow in volume in agreement with the modelling and tank experiments noted in Sect. 19.1. In the LaTTE region then, winds play a crucial role in determining the fate of material transported by the Hudson River to the inner shelf.

Choi and Wilkin (2007) also considered the influence of river discharge magnitude on the relative contribution of buoyancy and wind forcing to the momentum balance of the river plume. They found that relatively modest wind speeds of order 5 m/s are sufficient to overwhelm buoyancy forcing during typical non-freshet conditions.

It follows then that relatively short timescale variability in river discharge and weather conditions could lead to different dispersal patterns for the freshet in any

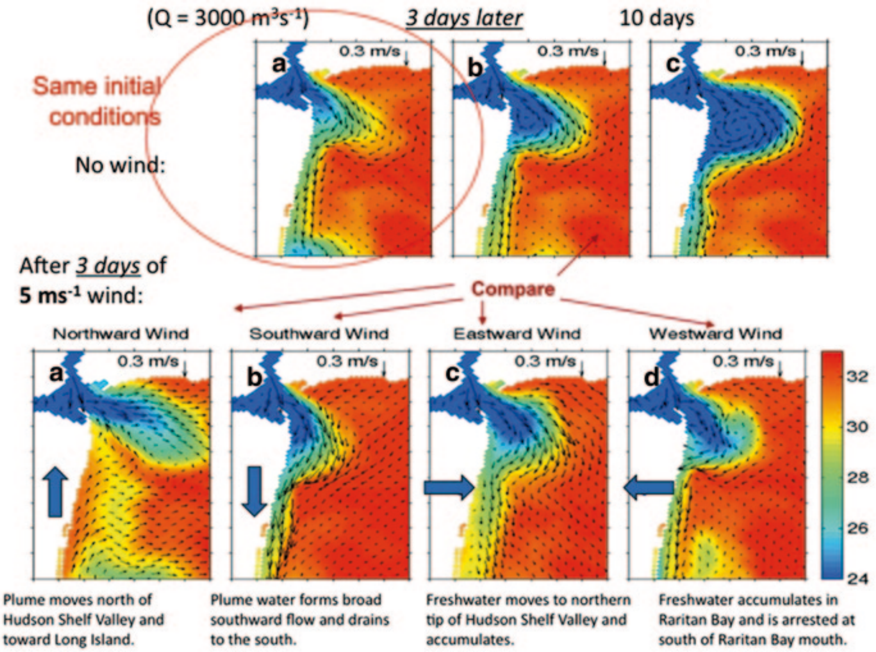

Fig. 19.5 Surface salinity of the Hudson River plume showing sensitivity of plume trajectory to wind during a high discharge event (3,000 m^3/s)

given year, and this was indeed found to be the case in the three LaTTE field seasons (Chant et al. 2008). In 2004, river waters were first transported southward in a modest coastal current, and then dispersed eastward in the surface Ekman layer associated with strong upwelling winds; 2005 was characterized by strong bulge formation and sea breeze activity as described above; while in 2006 unusually large river discharge fed a coastal current that flooded the New Jersey inner shelf with low salinity water, but this flow subsequently detached from the coast leading to significant across-shelf transport in the region south of the Hudson Shelf valley.

19.3.2 Shelf-Wide Transport and Dispersal Pathways

The preceding studies revealed that while some processes act to trap river plume water near the apex of the NYB (i.e. the recirculating bulge, and coastal current flow reversals) others disperse it widely (i.e. fast coastal currents and offshore wind-driven Ekman transport). Therefore the duration that river source waters dwell in the vicinity of the coastline can be quite variable, and questions arise as to where these waters eventually go.

To examine the ultimate fate of Hudson River source waters on time scales much longer than the spring freshet, we conducted multi-year simulations using the same model configuration but with modified open boundary inflow/outflow transport conditions and meteorology forcing from NARR.

The open boundary conditions were adapted to acknowledge that on inter-annual timescales the mid and outer New Jersey shelf is flushed by a southwestward along-shelf mean flow. An analysis of long term current meter observations and the mean momentum balance (Lentz 2008) indicates the depth-averaged along-shelf current is roughly proportional to water depth; this provides a convenient relationship upon which to base the time mean boundary transports to which we add the tidally varying currents.

The modelled mean circulation for 2005–2006 (Zhang et al. 2009a) is shown in Fig. 19.6. Buoyancy input from the Hudson River dominates flow in the apex of the NYB by driving the anticyclonic recirculation (a local maximum in sea surface height, SSH) associated with the low salinity bulge. This feature is sustained in the annual mean because it is the consequence not only of the spring freshet but also

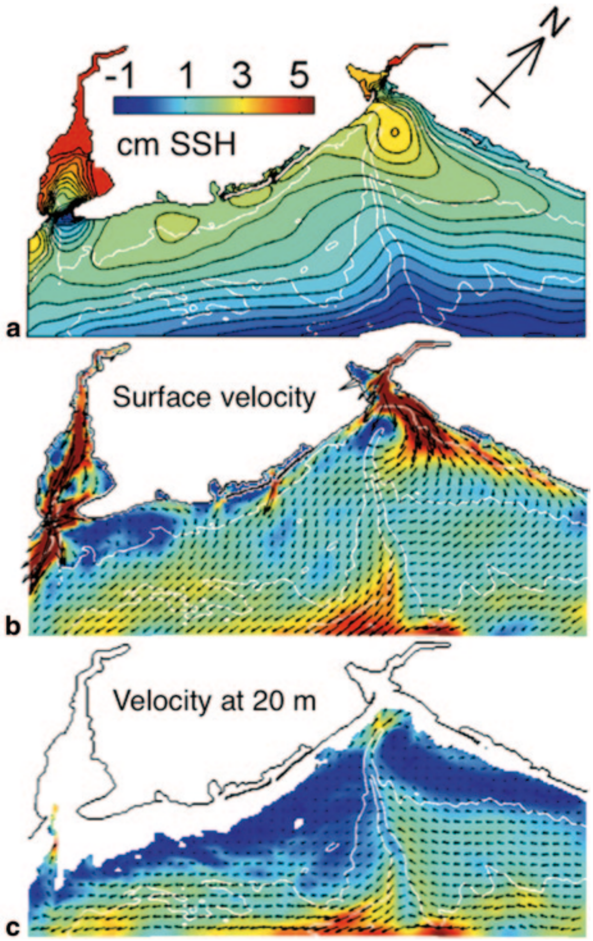

Fig. 19.6 Mean SSH (sea surface height) contours (**a,** *top*), and velocity at sea surface (**b,** *centre*) and 20-m depth (**c,** *bottom*) over the 2-year period 2005–2006

of high discharge events that can occur throughout the year. In the 3 years of the LaTTE program, the peak discharge actually occurred in July 2006 following heavy rains across all of New York State.

Transport is eastward along the Long Island coast, but this current ultimately detaches from the coast and reverses in the face of the mean flow that enters from the eastern open boundary.

On the mid to outer shelf the flow is to the southwest, largely parallel to isobaths, and deflected by the Hudson Shelf Valley as evidenced by the currents at 20 m (Fig. 19.6c). The influence of the valley extends throughout the water column and affects SSH. In the very apex of NYB the flow at 20 m is toward New York Harbor, indicating that the HSV serves as a conduit for shoreward flow that is vertically mixed and entrained into the estuary outflow and bulge recirculation. Away from the coast the surface currents (Fig. 19.6b) are dominated by southward wind-driven Ekman flow.

A New Jersey coastal current is not readily apparent in the annual mean. Zhang et al. (2009a) show it is prominent in spring and fall, moderate in winter, but overwhelmed by upwelling winds in the summer.

To avoid the ambiguity of reference salinity in lengthy simulations and to distinguish the Hudson River from other freshwater sources, Zhang et al. (2009a) introduce a passive tracer with unit concentration in the modelled Hudson River source and follow it to obtain an unambiguous measure of the dispersal pathways. Figure 19.7 shows the flux of Hudson River source water identified by its tracer signature across a set of arcs centred on the Harbor entrance. The qualitative features noted above are again evident. The New Jersey coastal current is clearly very tightly trapped against the coast, which partly explains why it is not conspicuous in Fig. 19.6a, b. Figure 19.7 quantifies the volume transports across sectors of the

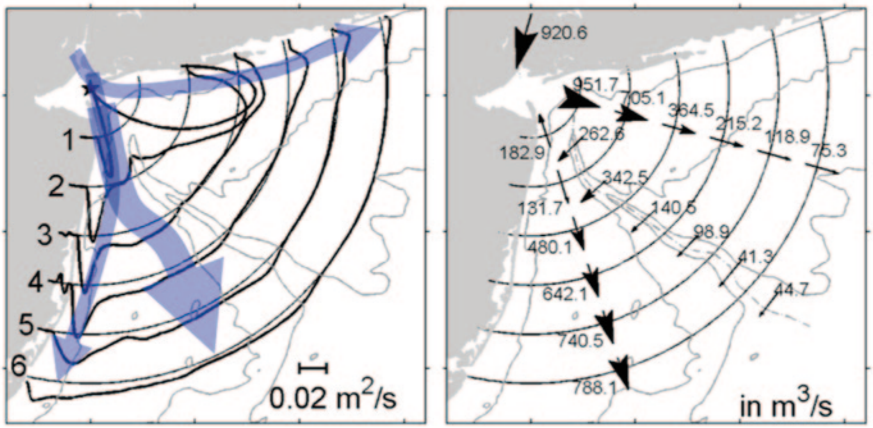

Fig. 19.7 *Left*: Two-year averaged, vertically integrated freshwater flux (*thick black lines*) across arcs of radius 20, 40, 60, 80, 100, and 120 km (numbered *1–6*) centred at the entrance to New York Harbor (*star*). *Right*: Freshwater transport (m^3/s) across the segments of the arcs on either side of the Hudson Shelf Valley (*gray dashed–dotted line*), and across the valley itself

arcs split at the HSV. In this 2-year mean, we see that river discharge is entirely to the shelf north of the HSV but that the majority of this flow subsequently crosses the valley within the general region of the recirculating bulge. Once south of the valley, the outflow is partitioned between the coastal current and a weaker but much broader across-shelf pathway guided by the south flank of the HSV. The latter current feature has been noted from HF radar surface current observations (Castelao et al. 2008). Despite initially entering the coastal ocean along the New York coast, the Hudson River discharge is thus ultimately dispersed to the mid and outer shelf on the south side of the Hudson Shelf Valley.

Biogeochemical observations during LaTTE (Moline et al. 2008) support the notion that the coastal current is typically supplied with biogeochemically processed water that has circulated around the bulge's perimeter rather than newly discharged water from the estuary.

In an example of the type of controlled dynamical analysis one can conduct with a model, Zhang et al. (2009a) separately withdrew individual forcing processes to examine the effect of each on the circulation. Their results are shown in Fig. 19.8, which should be compared to Fig. 19.6a, b for the full physics solution.

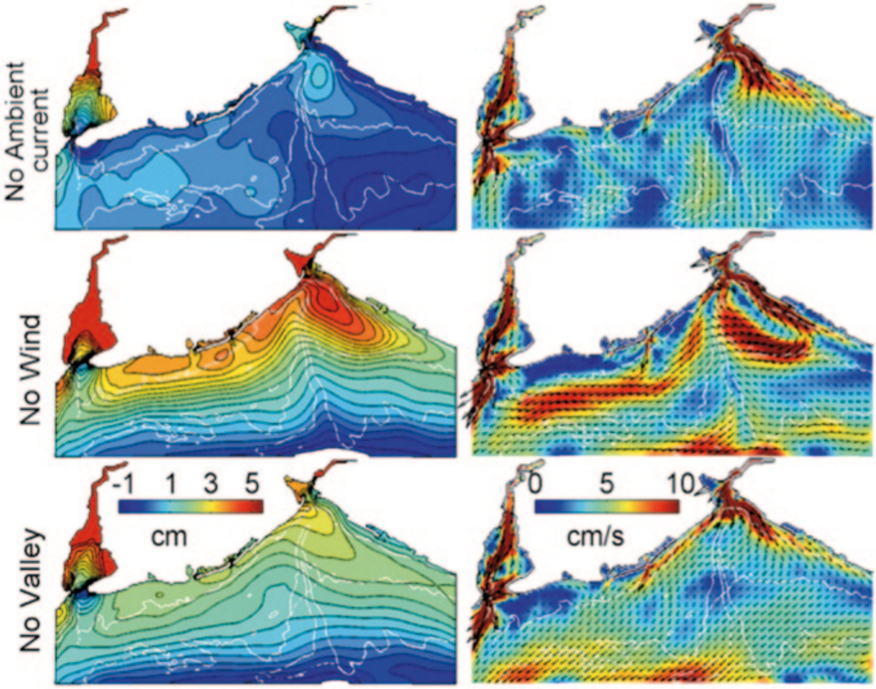

Fig. 19.8 Mean SSH (sea surface height) contours (*left*) and surface currents and magnitude (*right*) over the 2-year period 2005–2006 for three simulations with changes to the full physics configuration shown in Fig. 19.6. *Top row*: Outer shelf boundary forcing removed. *Middle row*: Wind stress removed. *Bottom row*: Bathymetry of Hudson Shelf Valley filled in

Without the remotely forced along-shelf mean flow the bulge recirculation remains, but the across-shelf surface flow is more eastward being the result solely of Ekman transport and not combined with geostrophic southward flow.

In the absence of wind forcing the bulge is more intense, in accordance with the results of Fong and Geyer (2002) who found that along-shore transport driven by wind arrests continuous growth of bulge recirculation. As in the full physics case, part of this recirculation feeds flow on the south side of the HSV, but without winds the downstream flow is largely at mid-shelf parallel to the coast and does not disperse to the outer shelf.

Zhang et al. (2009a) explored whether the Hudson Shelf Valley impacts circulation by simply removing the valley from the model bathymetry. Figure 19.8 shows that in the No Valley case the SSH signature of the bulge is substantially weakened, and surface velocity shows far more of the estuary outflow enters the NJ coastal current.

In an extension of their passive tracer approach for following Hudson River waters, Zhang et al. (2010a) employ the concept of 'mean age' (Deleersnijder et al. 2001) to determine the transit time from river source to shelf ocean. If we denote the equation governing the transport of a passive tracer with concentration C by

$$\frac{\partial C}{\partial t} + \nabla \cdot (\mathbf{u}C) = \nabla \cdot (\mathbf{K} \cdot \nabla C)$$

then an 'age concentration' tracer α can be introduced satisfying

$$\frac{\partial \alpha}{\partial t} + \nabla \cdot (\mathbf{u}\alpha) = \nabla \cdot (\mathbf{K} \cdot \nabla \alpha) + C$$

where the last term on the right causes α to increase in proportion to the concentration of river source water present. The concentration of the tracers in the river source are $C=1$ and $\alpha=0$. The 'mean age' (Deleersnijder et al. 2001) is given by $a(\mathbf{x},t) = \alpha(\mathbf{x},t)/C(\mathbf{x},t)$ and describes the duration it has been *on average* since the waters at a given position and time $(\mathbf{x},t)$ entered the domain at the river source. Figure 19.9 illustrates how mean age evolves in a simulation where the river tracer release commenced on 13 March. It takes some 4–5 days for river water to reach the bulge circulation, and water on the southwest side of the bulge is clearly older than water to the north. On March 18 an increase in river discharge a few days previously introduces a surge of younger water that forms a sharp gradient in mean age across the western edge of bulge. In 7 days none of the river water has escaped the bulge. In regions the passive tracer has not reached the mean age is undefined.

Zhang et al. (2010a) show that mean age patterns in the 2005 LaTTE period mimic an age proxy determined from a ratio of satellite observed water leaving radiance that expresses the relative concentration of CDOM (Coloured Dissolved Organic Matter) to phytoplankton. CDOM is the dominant optical constituent in river source waters and has high absorption at 490 nm but it subsequently photodegrades whereas phytoplankton concentration (with chlorophyll-*a* spectral peak at 670 nm) increases as the plume ages, so the CDOM decrease and phytoplankton

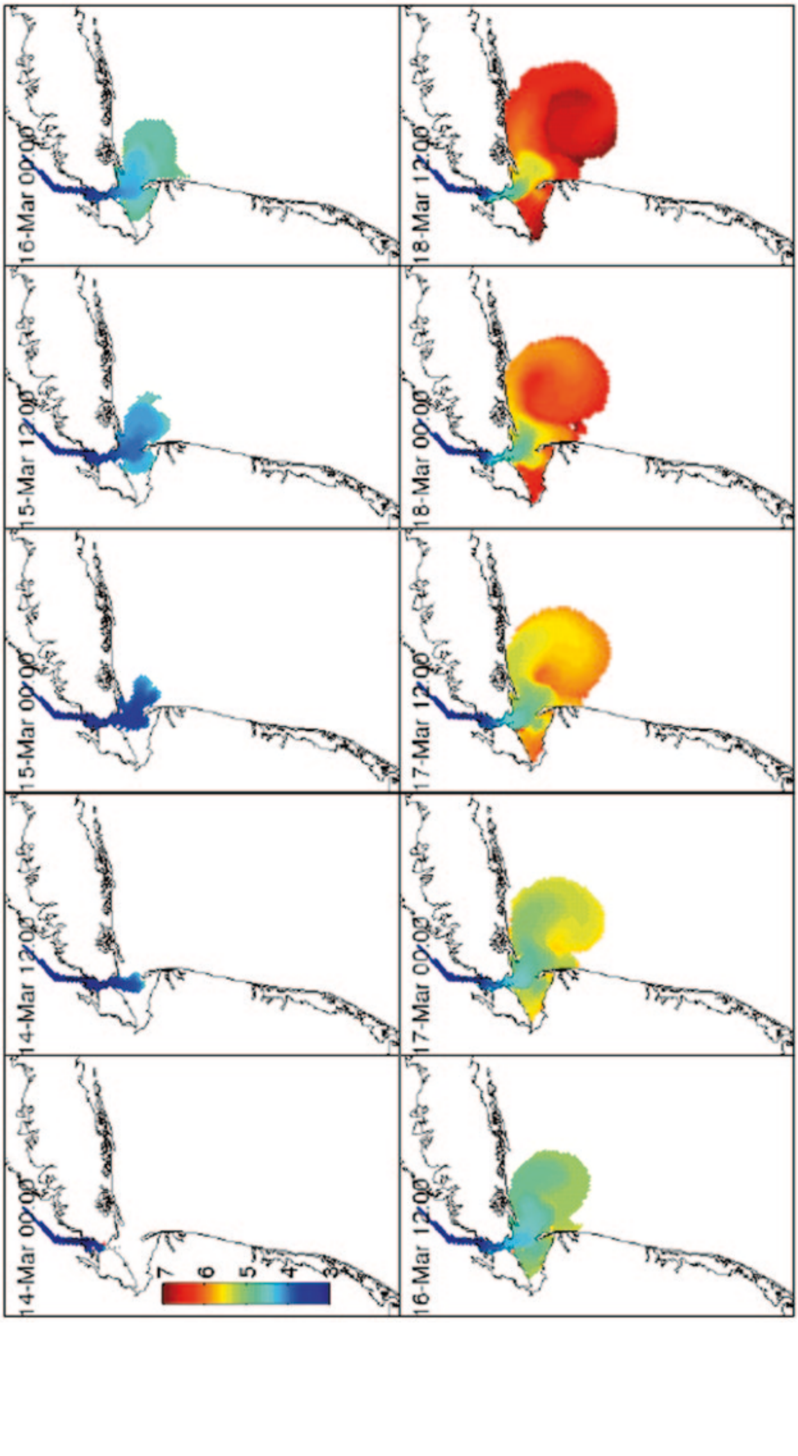

Fig. 19.9 Modelled mean age (colour scale in days) for a simulation commencing on 13-March

increase produces a spectral shift in the remote sensing reflectance. Zhang et al. (2010a) found a robust empirical relationship between simulated age and observed reflectance ratio that has promise for estimating river water age in the NYB—a property of relevance to rates of biogeochemical transformation of river source organic matter and pollutants (Moline et al. 2008).

19.3.3 Data Assimilation and Observing System Design

The NYB is among the most densely observed coastal oceans in the world, having been the target of pioneering deployments of new observing instruments including a cabled observatory (Glenn and Schofield 2003), surface current measuring high-frequency radar (CODAR) (Kohut et al. 2006) and autonomous underwater vehicles (gliders) (Schofield et al. 2007). To these systems and regular satellite imagery, LaTTE added moorings, surface drifters, and towed undulating CTD instruments deployed from the research vessels *Cape Hatteras* and *Oceanus*. These data and the sustained operation of much of the instrumentation make the NYB an attractive location to explore the integration of observation and modelling capabilities through advanced data assimilation.

The locations of LaTTE 2006 *in situ* observations are shown in Fig. 19.1. CODAR coverage was near complete from Long Island to Delaware Bay and out to the 40 m isobath, with some gaps in the apex of NYB. There were satellite SST data from approximately four passes each day, cloudiness permitting.

Here we use data assimilation (DA) for state estimation; namely, to obtain an analysis for initializing subsequent forecasts so as to enhance short-term forecast skill. This approach is common practise in Numerical Weather Prediction (NWP). We use a 4-dimensional (time-dependent) variational (4DVAR) method for DA, which is one among many possible approaches but again one that draws on experience in advanced NWP. We use the so-called Incremental Strong Constraint (IS4DVAR) formulation (Courtier et al. 1994) whose implementation in ROMS is described in detail elsewhere (Broquet et al. 2009; Powell et al. 2008; Zhang et al. 2010b).

IS4DVAR minimizes a cost function expressing the mismatch between observations and the model state at each observation location and time, summed over an analysis interval. Our implementation uses a 3-day interval—short enough for the linearization assumption of the incremental formulation to hold, but long enough for the model physics (embodied in the adjoint and tangent linear models) to exert the strong constraint interconnection (covariance) of model state variables. The control variables of the DA are the initial conditions to each 3-day analysis, with the intervals overlapped so as to generate initial conditions each day to launch a new 72-h forecast.

IS4DVAR does not explicitly allow for model error as would, for example, representer-based or weak constraint 4DVAR (Bennett 2002; Courtier 1997). Errors in model physics, numerics, meteorological forcing and boundary conditions are incorporated into the model background error covariance. The observations are assigned error variances appropriate to the observation source.

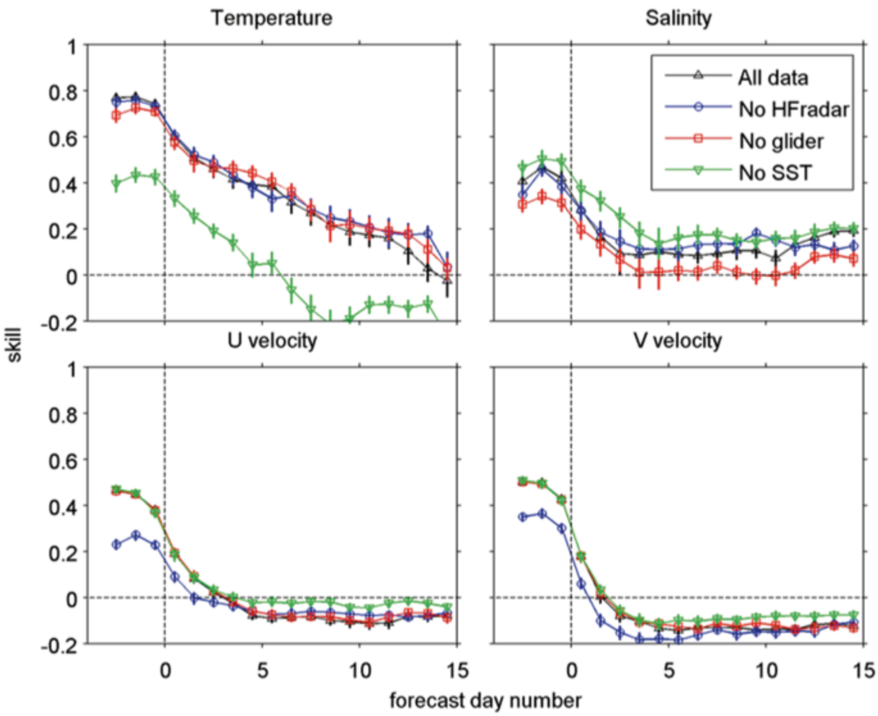

Fig. 19.10 Added skill introduced by data assimilation for analysis and forecast periods for individual forecast variables. Results are ensemble average of 60 forecast cycles. Vertical bars on symbols indicate 95% confidence intervals. Vertical *dashed lines* denote the boundary between analysis window and forecast window

Our reanalysis was conducted after the data were gathered, but we describe a DA and forecast system that could have operated in real-time because glider and vessel data are telemetered to shore. Lessons learned from this study on practical issues of data timeliness, quality control, and configuration of the IS4DVAR algorithm on a broad, shallow shelf, with significant tides have been incorporated in the Experimental System for Predicting Shelf and Slope Optics (ESPreSSO[1]) that currently runs operationally for the Mid-Atlantic Bight and encompasses the LaTTE domain.

The value that DA adds to the forecast system can be evaluated by considering how well observations are forecast prior to their assimilation on later analysis cycles. We quantify this with a DA skill metric

$$S = 1 - (RMS_{after\ DA}/RMS_{before\ DA})$$

where *RMS* is the root-mean-square of model-observation mismatch weighted by observational error. For 60 days of simulation spanning LaTTE 2006 we have multiple 1-day, 2-day, etc. forecasts that may be combined into ensemble estimates for increasing forecast window. Figure 19.10 shows the skill for different variables

[1] ESPreSSO results may be viewed at www.myroms.org/applications/espresso.

when all available data are assimilated (black lines), and when selected data categories are withdrawn from the analysis step (coloured lines). Forecast times less than zero are in the analysis interval, and show the ability of the system to match observations and model prior to launching the forecast. As forecast time proceeds the skill declines, but note that $S=0$ does not say the model has no utility at all, merely that assimilation no longer *adds* any advantage to the model predictive skill. For temperature, DA adds skill to the forecast out to some 10–15 days, for salinity 5–10 days, and for velocity about 2–3 days. The more rapid decline in skill for velocity compared to tracers reflects the shorter autocorrelation timescales for velocity and that it is inherently less predictable.

Not surprisingly, withdrawing data diminishes skill for that variable, i.e. without HF-radar data the velocity skill falls, and without satellite SST the temperature skill falls. However, there can be a modest increase in skill for other variables, e.g. salinity forecast skill is slightly higher when SST are not assimilated. We interpret this as the DA system not needing to reconcile glider and satellite temperatures and having rather more freedom to adjust initial salinity to improve the salinity analysis; recall that all the variables are dynamically linked through the strong constraint of the adjoint and tangent linear models. Overall, skill is best when all data are included, and therefore diversity in the data sources is to be preferred.

Details of the ROMS IS4DVAR configuration for LaTTE with respect to background error covariance and the pre-processing of observations are discussed by Zhang et al. (2010b), who also examine surface versus subsurface skill, and the influence of errors in surface forcing on system performance.

A further application of variational methods in ocean modelling is adjoint sensitivity analysis, which allows some inference of observation locations that are likely to have greater impact on the DA analysis. Studies using adjoint sensitivity in coastal oceanography are still relatively few compared to meteorology and mesoscale and gyre-scale oceanography, but Moore et al. (2009) examine how upwelling, eddy kinetic energy and baroclinic instability in the California Current are affected by surface forcing on seasonal timescales. Here we present some results due to Zhang et al. (2009b) who use the adjoint of the LaTTE model to reveal the spatial and temporal distribution of ocean model state variables that are "dynamically upstream" to features of coastal circulation.

A characteristic of New Jersey coastal ocean dynamics is that significant SST variability is driven by along-shore winds (Chant 2001; Münchow and Chant 2000). Zhang et al. (2009b) considered this process by introducing a scalar function that expresses SST anomaly variance averaged over a localized area adjacent to the coast

$$J = \frac{1}{2(t_2 - t_1)A} \int_{t_1}^{t_2} \int_A (T_s - \overline{T}_s)^2 dA dt,$$

where T_s is SST and $\overline{T}_s$ is its temporal mean; this definition considers temperature anomaly within an area A during a set time interval. Here, the time period is chosen to be the last three hours of the simulation time window. Defining J in quadratic form prevents the cancellation of positive and negative anomalies.

Temperature, salinity and velocity outside region A affect J through transport (advection and diffusion) and dynamics (baroclinic pressure gradients, stratification, turbulent mixing). Denoting the 4-dimensional ocean state (T, S, u, v, ζ) by a vector Φ, it can be shown that $\partial J/\partial\Phi$—representing the dependence of J on the ocean state—is the solution of the ROMS adjoint model integrated backward in time and forced by $\partial J/\partial T$ computed from the forward model. See Zhang et al. (2009b) for details. Although J is a scalar, $\partial J/\partial\Phi$ has the same dimension as Φ, i.e. the entire ocean state through time, which emphasizes that all the surrounding ocean can potentially project on to SST variance in A. This adjoint sensitivity concept can be grasped, qualitatively, from an example: Fig. 19.11 maps the sensitivity of J to surface temperature, i.e. $\partial J/\partial T$ at $z=0$, over the 3 days that precede the interval t_1 to t_2 over which J is defined, for the cases of downwelling and upwelling winds. The sequence proceeds backwards in time from day 3 to day 0. We have already demonstrated that southward (downwelling) winds favour coastal current formation, and for this case (Fig. 19.11, top row) the adjoint sensitivity advances from region A (delineated by the black box) back along the trajectory of the coastal current to New York Harbor. In the upwelling wind case (Fig. 19.11, bottom row), surface temperatures in preceding times have very little impact of SST variance in A. This is because the coastal current is not dynamically upstream in this situation; rather, surface temperatures depend more on source waters drawn from below the surface. The final panel on the right shows $\partial J/\partial T$ at $t=0$ along a vertical cross-section slightly south of region A, and confirms that J is sensitive to remote subsurface temperatures during upwelling. While these results have a ready qualitative interpretation, adjoint sensitivity quantifies the dependence and immediately indicates where "upstream" is. Zhang et al. (2009b) further quantify the relative importance of other state variables by contrasting the magnitude of $\partial J/\partial T$ with $\partial J/\partial S$, $\partial J/\partial u$, etc.

One can immediately see the potential for this information to assist observing system operation. By identifying the timing and location of ocean conditions having significant influence on the subsequent evolution of specific circulation features (characterized by some chosen J), adjoint sensitivity indicates where, when and what observations are likely to have greater impact in a 4DVAR assimilation system. In a companion paper, Zhang et al. (2010c) extend this approach using so-called *representers*, also based on variational methods, to examine the information content of a set of observations such as might be gathered routinely on a repeat transect occupied by an autonomous vehicle, or by a sustained cabled observatory.

19.4 Processes and Dynamics for Further Study

19.4.1 Air-Sea and Wave-Current Interaction

The results described above all utilize essentially the same model configuration options emphasized in Sect. 19.2, but the LaTTE program identified roles for some

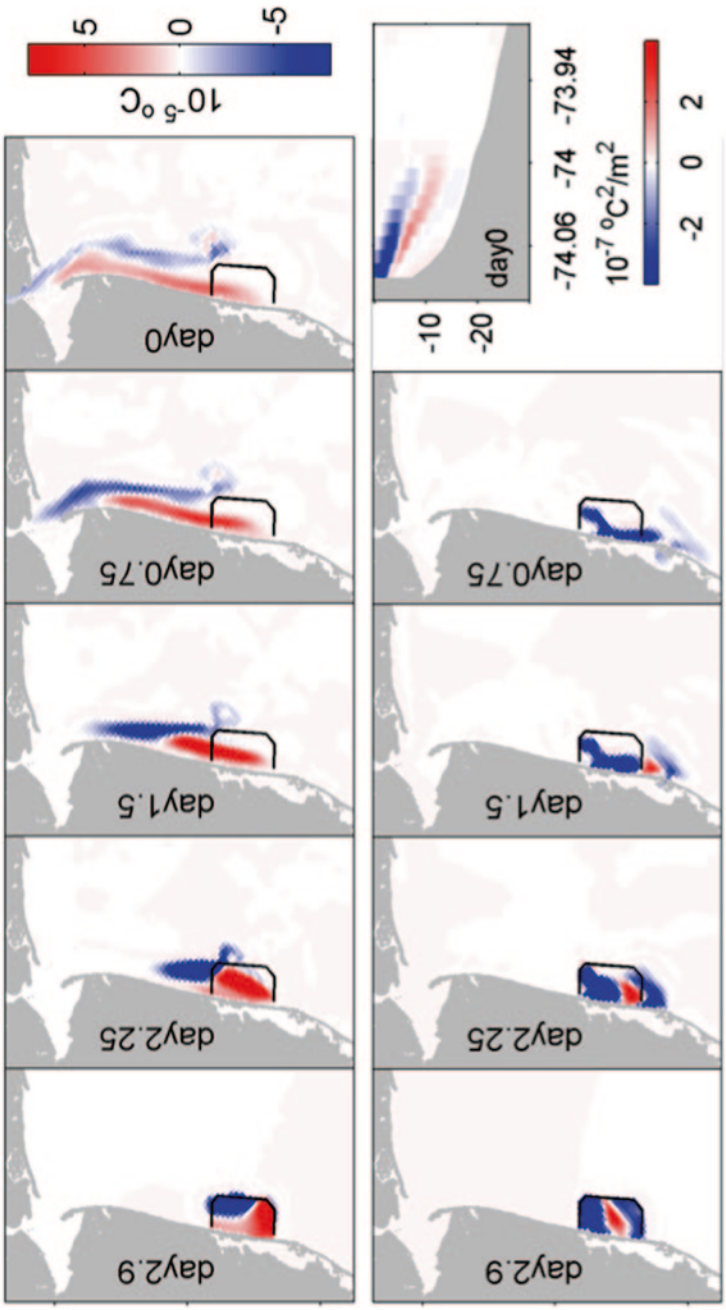

Fig. 19.11 Sensitivity of J to surface temperature at different times during the 3-day period. *Top row*: Southward down-welling winds. *Bottom row*: Northward upwelling winds. Panel at *right* shows sensitivity at day 0 (upwelling case) on a vertical section. (See the text for discussion)

dynamical processes that were not incorporated in the model physics employed here that are worthy of incorporation in future model-based studies.

In the NYB, sea-land-breeze system (SLBS) activity can be pronounced during spring (Hunter et al. 2007, 2010) when ocean temperatures are still cool but the land is warming. Since this is precisely the time of year when river discharge peaks with the spring freshet, atmosphere-ocean interactions fundamental to SLBS dynamics are likely important to achieving realistic simulations of the plume circulation. Furthermore, mid-summer SLBS activity further south on the Jersey Shore is influenced by SST changes associated with wind-driven coastal upwelling (Bowers 2004). Full synchronous coupling of ROMS with an atmospheric forecast model has the potential to improve both ocean and atmosphere forecasts when SLBS conditions occur, and this capability has been added to ROMS by coupling to the COAMPS (Coupled Ocean Atmosphere Prediction System) (Warner et al. 2008b) and WRF (Weather Research and Forecasting) models.

Surface wind waves mediate air-sea interaction by modifying drag and hence net momentum exchange, plus surface wave radiation stress, Stokes drift and wave-current interaction processes in the bottom boundary layer drag are important in the ocean momentum balance itself. It was noted in Sect. 19.2.4 that these dynamical processes are now incorporated in ROMS, including the option to synchronously couple with the SWAN wave model. Studies of the Hudson plume that employed higher resolution than the 1 km grid used here and placed greater emphasis on processes in shallow waters near the coast (inside the 15-m isobath) or at the leading edge of the plume, may demonstrate that inclusion of these dynamics are important to faithful simulation of the plume evolution.

19.4.2 Ecosystem-Optics and Heating Interaction

Like most coastal ocean models, ROMS assumes constant absorption coefficients for shortwave radiation (Paulson and Simpson 1977) leading to a vertical exponential decay in internal solar heating. But optical properties of coastal waters can be far from spatially uniform, and observations during LaTTE exhibited distinct regions of turbid water associated with the river plume, motivating Cahill et al. (2008) to use the EcoSim model (Sect. 19.2.4) to examine coupling between shortwave radiation attenuation, buoyancy and photosynthesis. The solar heating parameterization was modified to make shortwave absorption dependent on the concentration of river source freshwater as a proxy for increased attenuation in the plume. The feedback between solar heating and vertical stratification was sufficient to modify the buoyancy driven circulation and mixed layer depth. This in turn raised concentrations of chlorophyll, detritus and coloured dissolved organic matter (CDOM) in the upper water column increasing attenuation of photosynthetically active radiation (PAR) and further impacting phytoplankton growth.

Simulations with full ecosystem-absorption-heating feedback (i.e. spectrally resolved 3-dimensional radiative absorption determined by optically active constituents in the water column) have shown differences in simulated temperature can be as much as 2°C warmer at the surface, and correspondingly cooler some 10 m deeper, in the Hudson River plume. The associated changes in plume trajectory and ecosystem dynamics alter net export of particulate matter to mid shelf waters. Incorporating these optical properties into the 4-dimensional ocean state is a natural future step to enhance data assimilation in coastal ocean models.

19.5 Summary

We have described a series of model-based studies of circulation in the New York Bight region that utilize data from a sustained coastal ocean observing system complemented by extensive in situ observations from the LaTTE project.

Observations are used to evaluate the performance of traditional forward simulations where the model formulation is treated as an initial and boundary value problem. Circulation on the New Jersey inner shelf, and especially within the NYB, is strongly locally driven and direct forward simulations with ROMS are quite skilful—a result we attribute to the model being comprehensive and accurate in the suite of dynamical processes it represents and the numerical algorithms it employs, suitably configured in terms of bathymetric and coastline detail, and driven by meteorological, hydrological and tidal forcing with sufficient resolution and accuracy.

Using forward model simulations we have seen that the NYB circulation is particularly responsive to wind forcing, how buoyancy dynamics contribute to the retention of river source waters in the NYB apex through formation of a persistent anti-cyclonic recirculation, and that the model can be used to quantify this residence time by incorporating an age tracer. Long simulations reveal the pathways by which Hudson River borne material is ultimately dispersed across the New Jersey shelf.

Moving beyond traditional forward simulations, we have illustrated how coastal models are now being increasingly integrated with the growing network of regional coastal ocean observing systems. The creation of variational complements to the ROMS nonlinear forward model (i.e. the ROMS adjoint and tangent linear models) has enabled the implementation of 4-dimensional variational data assimilation in coastal ocean analysis with an attendant improvement in forecast skill. Variational-based methods have further capabilities beyond data assimilation, through helping inform adaptive sampling strategies and observing system design targeted at improving predictive skill.

References

Avicola G, Huq P (2003) The role of outflow geometry in the formation of the recirculating bulge region in coastal buoyant outflows. J Mar Res 61:411–434

Bennett AF (2002) Inverse modeling of the ocean and atmosphere. Cambridge University Press, Cambridge, p 234

Bissett WP, Walsh JJ, Dieterle DA, Carder KL (1999) Carbon cycling in the upper waters of the Sargasso sea: I. Numerical simulation of differential carbon and nitrogen fluxes. Deep Sea Res Part I Oceanogr Res Pap 46:205–269

Booij N, Ris RC, Holthuijsen LH (1999) A third-generation wave model for coastal regions. Part I: model description and validation. J Geophys Res 104(C4):7649–7666

Bowers L (2004) The effect of sea surface temperature on sea breeze dynamics along the coast of New Jersey. M.S. thesis, Rutgers University, New Brunswick

Broquet G, Edwards CA, Moore AM, Powell BS, Veneziani M, Doyle JD (2009) Application of 4D-variational data assimilation to the California current system. Dyn Atmos Oceans 48:69–92

Cahill B, Schofield O, Chant R, Wilkin J, Hunter E, Glenn S, Bissett P (2008) Dynamics of turbid buoyant plumes and the feedbacks on near-shore biogeochemistry and physics. Geophys Res Lett 35, L10605. doi:10.1029/2008GL033595

Castelao RM, Schofield O, Glenn S, Chant RJ, Kohut J (2008) Cross-shelf transport of fresh water on the New Jersey shelf. J Geophys Res 113, C07017. doi:10.1029/2007JC004241

Chant RJ (2001) Evolution of near-inertial waves during an upwelling event on the New Jersey inner shelf. J Phys Oceanogr 31:746–764

Chant RJ, Wilkin J, Zhang W, Choi B-J, Hunter E, Castelao R, Glenn S, Jurisa J, Schofield O, Houghton R, Kohut J, Frazer TK, Moline MA (2008) Dispersal of the Hudson River plume in the New York Bight: synthesis of observational and numerical studies during LaTTE. Oceanography 21(4):148–161

Chapman DC (1985) Numerical treatment of cross-shelf open boundaries in a barotropic ocean model. J Phys Oceanogr 15:1060–1075

Choi B-J, Wilkin JL (2007) The effect of wind on the dispersal of the Hudson River plume. J Phys Oceanogr 37:1878–1897

Courtier P, Thépaut J-N, Hollingsworth A (1994) A strategy for operational implementation of 4DVAR using an incremental approach. Q J R Meteorol Soc 120:1367–1388

Courtier P (1997) Dual formulation of four-dimensional variational assimilation. Q J R Meteorol Soc 123:2449–2461

Deleersnijder E, Campin J-M, Delhez EJM (2001) The concept of age in marine modelling: I. Theory and preliminary model results. J Mar Syst 28:229–267

Durski S, Glenn SM, Haidvogel D (2004) Vertical mixing schemes in the coastal ocean: comparison of the level 2.5 Mellor-Yamada scheme with an enhanced version of the K-profile parameterization. J Geophys Res 109, C01015. doi:10.1029/2002JC001702

Fairall CW, Bradley EF, Hare JE, Grachev AA, Edson J (2003) Bulk parameterization of air–sea fluxes: updates and verification for the COARE algorithm. J Climate 16:571–591

Flather RA (1976) A tidal model of the northwest European continental shelf. Memoires Soc R Sci Liege Ser 6(10):141–164

Fong DA, Geyer WR (2002) The alongshore transport of freshwater in a surface-trapped river plume. J Phys Oceanogr 32:957–972

Foti G (2007) The Hudson River plume: utilizing an ocean model and field observations to predict and analyze physical processes that affect the freshwater transport. M.S. Thesis, Rutgers University, New Brunswick

Glenn SM, Schofield O (2003) Observing the oceans from the COOLroom: our history, experience, and opinions. Oceanography 16:37–52

Haidvogel D, Arango H, Budgell W, Cornuelle B, Curchitser E, Di Lorenzo E, Fennel K, Geyer WR, Hermann A, Lanerolle L, Levin J, McWilliams JC, Miller A, Moore AM, Powell TM, Shchepetkin AF, Sherwood C, Signell R, Warner JC, Wilkin J (2008) Ocean forecasting in terrain-following coordinates: formulation and skill assessment of the regional ocean modeling system. J Comput Phys 227:3595–3624

Higdon RL, de Szoeke RA (1997) Barotropic-baroclinic time splitting for ocean circulation modeling. J Comput Phys 135:31–53

Hill AE (1998) Buoyancy effects in coastal and shelf seas. In: Robinson AR, Brink KH (eds) The sea. The global coastal ocean, vol 10. Harvard University Press, London, pp 21–62

Horner-Devine AR, Fong DA, Monismith SG, Maxworthy T (2006) Laboratory experiments simulating a coastal river outflow. J Fluid Mech 555:203–232
Hunter E, Chant R, Bowers L, Glenn S, Kohut J (2007) Spatial and temporal variability of diurnal wind forcing in the coastal ocean. Geophys Res Lett 34, L03607. doi:10.1029/2006GL028945
Hunter E, Chant R, Wilkin J, Kohut J (2010) High-frequency forcing and sub-tidal response of the Hudson River plume. J Geophys Res 115, C07012. doi:10.1029/2009JC005620
Janjic ZL (2004) The NCEP WRF core. 20th Conference on Weather Analysis and Forecasting/16th Conference on Numerical Weather Prediction, Seattle. Am Meteorol Soc. http://ams.confex.com/ams/84Annual/techprogram/paper_70036.htm
Kohut JT, Roarty HJ, Glenn SM (2006) Characterizing observed environmental variability with HF doppler radar surface current mappers and acoustic doppler current profilers: environmental variability in the coastal ocean. IEEE J Ocean Eng 31:876–884
Large WG, McWilliams JC, Doney SC (1994) A review and model with a nonlocal boundary layer parameterization. Rev Geophys 32:363–403
Lentz SJ (2008) Observations and a model of the mean circulation over the Middle Atlantic Bight continental shelf. J Phys Oceanogr 38:1203–1221
Mellor GL, Yamada T (1982) Development of a turbulence closure model for geophysical fluid problems. Rev Geophys Sp Phys 20:851–875
Mesinger F, DiMego G, Kalnay E, Mitchell K, Shafran P, Ebisuzaki W, Jovic D, Woollen J, Rogers E, Berbery E, Ek M, Fan Y, Grumbine R, Higgins W, Li H, Lin Y, Manikin G, Parrish D, Shi W (2006) North American regional reanalysis. B Am Meteorol Soc 87:343–360
Moline MA, Frazer TK, Chant R, Glenn S, Jacoby CA, Reinfelder JR, Yost J, Zhou M, Schofield O (2008) Biological responses in a dynamic Buoyant River plume. Oceanography 21(4):70–89
Moore AM, Arango HG, Di Lorenzo E, Miller AJ, Cornuelle BD (2009) An adjoint sensitivity analysis of the southern California Current circulation and ecosystem. J Phys Oceanogr 39:702–720
Mukai AY, Westerink JJ, Luettich RA, Mark D (2002) Eastcoast 2001, a tidal constituent database for the western North Atlantic, Gulf of Mexico and Caribbean Sea. Tech. Rep. ERDC/CHL TR-02-24, p 196
Münchow A, Chant RJ (2000) Kinematics of inner shelf motion during the summer stratified season off New Jersey. J Phys Oceanogr 30:247–268
Nof D, Pichevin T (2001) The ballooning of outflows. J Phys Oceanogr 31:3045–3058
Paulson CA, Simpson JJ (1977) Irradiance measurements in the upper ocean. J Phys Oceanogr 7:952–956
Powell TM, Lewis CVW, Curchister EN, Haidvogel DB, Hermann AJ, Dobbins EL (2006) Results from a three-dimensional, nested biological-physical model of the California Current system and comparisons with statistics from satellite imagery. J Geophys Res 111, C07018. doi:10.1029/2004JC002506
Powell BS, Arango HG, Moore AM, Di Lorenzo E, Milliff RF, Foley D (2008) 4DVAR data assimilation in the Intra-Americas sea with the regional ocean modeling system (ROMS). Ocean Model 25:173–188
Schofield O, Bosch J, Glenn SM, Kirkpatrick G, Kerfoot J, Moline MA, Oliver M, Bissett P (2007) Bio-optics in integrated ocean observing networks: potential for studying harmful algal blooms. In: Babin M, Roesler C, Cullen JJ (eds) Real time coastal observing systems for ecosystem dynamics and harmful algal blooms. UNESCO, Valencia, pp 85–108
Shchepetkin A, McWilliams J (2005) The regional oceanic modeling system (ROMS): a split-explicit, free-surface, topography-following-coordinate oceanic model. Ocean Model 9:347–404
Shchepetkin A, McWilliams J (2009a) Computational kernel algorithms for fine-scale, multi-process, long-term oceanic simulations. In: Temam R, Tribbia J (Guest eds) Computational methods for the ocean and the atmosphere. In: Ciarlet PG (ed) Handbook of numerical analysis, vol 14. Elsevier, Amsterdam, pp 119–182. doi:10.1016/S1570-8659(08)01202-0
Shchepetkin A, McWilliams J (2009b) Correction and commentary for ocean forecasting in terrain-following coordinates: formulation and skill assessment of the regional ocean modeling

system. J Comp Phys 228:8985–9000 (by Haidvogel et al., J Comp Phys 227:3595–3624). doi:10.1016/j.jcp.2009.09.002

Smolarkiewicz PK (1984) A fully multidimensional positive-definite advection transport algorithm with small implicit diffusion. J Comput Phys 54:325–362

Umlauf L, Burchard H (2003) A generic length-scale equation for geophysical turbulence models. J Mar Res 61:235–265

Warner J, Sherwood C, Arango H, Signell R (2005) Performance of four turbulence closure models implemented using a generic length scale method. Ocean Model 8:81–113

Warner JC, Sherwood CR, Signell RP, Harris CK, Arango HG (2008a) Development of a three-dimensional, regional, coupled wave, current, and sediment-transport model. Comput Geosci 34:1284–1306. doi:10.1016/j.cageo.2008.02.012

Warner JC, Perlin N, Skyllingstad ED (2008b) Using the Model Coupling Toolkit to couple earth system models. Environ Model Softw 23:1240–1249

Wijesekera HW, Allen JS, Newberger PA (2003) Modeling study of turbulent mixing over the continental shelf: comparison of turbulent closure schemes. J Geophys Res 108(C3):3103

Yankovsky AE, Chapman DC (1997) A simple theory for the fate of buoyant coastal discharges. J Phys Oceanogr 27:1386–1401

Zhang W, Wilkin J, Chant R (2009a) Modeling the pathways and mean dynamics of river plume dispersal in New York Bight. J Phys Oceanogr 39:1167–1183. doi:10.1175/2008JPO4082.1

Zhang W, Wilkin J, Levin J, Arango H (2009b) An adjoint sensitivity study of buoyancy- and wind-driven circulation on the New Jersey inner shelf. J Phys Oceanogr 39:1652–1668. doi:10.1175/2009JPO4050.1

Zhang W, Wilkin J, Schofield O (2010a) Simulation of water age and residence time in the New York Bight. J Phys Oceanogr. doi:10.1175/2009JPO4249.1

Zhang W, Wilkin J, Arango H (2010b) Towards an integrated observation and modeling system in the New York Bight using variational methods. Part I: 4DVAR data assimilation. Ocean Model 35:119–133. doi:10.1016/j.ocemod.2010.08.003

Zhang W, Wilkin J, Levin J (2010c) Towards an integrated observation and modeling system in the New York Bight using variational methods. Part II: representer-based observing system design. Ocean Model 35:134–145. doi:10.1016/j.ocemod.2010.06.006